

Molecular Anchors for Self-Assembled Monolayers on ZnO: A Direct Comparison of the Thiol and Phosphonic Acid Moieties

Craig L. Perkins

National Renewable Energy Laboratory, Golden, Colorado

Received: June 26, 2009; Revised Manuscript Received: September 10, 2009

Two of the most promising schemes for attaching organic molecules to metal oxides are based on the chemistry of the thiol and phosphonic acid moieties. We have made a direct comparison of the efficacy of these two molecular anchors on zinc oxide by comparing the chemical and physical properties of *n*-hexane derivatives of both. The surface properties of polycrystalline ZnO thin films and ZnO(0001)-O crystals modified with 1-hexanethiol and 1-hexanephosphonic acid were examined with a novel quartz crystal microbalance (QCM)-based flow cell reactor, angle-resolved and temperature-dependent photoelectron spectroscopy, and contact angle measurements. A means of using ammonium chloride as a probe of molecule-ZnO interactions is introduced and used to ascertain the relative quality of self-assembled monolayers (SAMs) based on thiols and phosphonic acids. QCM data shows that a phosphonic acid-anchored alkyl chain only six carbons long can provide significant corrosion protection for ZnO against Brønsted acids, reducing the etch rate relative to the bare ZnO surface by a factor of more than nine. In contrast, we find that monolayers from the analogous molecule hexanethiol are more defective as revealed by their higher ionic permeability and lower hydrophobicity. Substrate attenuation X-ray photoelectron spectroscopy (XPS) experiments were used to determine the thickness of SAMs formed by the two hexane derivatives and it was found that SAMs from phosphonic acids were approximately twice as thick as those formed by hexanethiol. The thermal stability of the two linking groups was also explored and we find that previous claims of highly stable alkanethiolate monolayers on ZnO are suspect. Taken as a whole, our results indicate that the phosphonic acid moiety is preferred over thiols for the attachment of short alkyl groups to ZnO.

Introduction

The seemingly infinite structural variability of organic molecules makes them attractive functional materials because of the wide latitude it provides to chemists seeking specific material properties. This is one of the driving forces behind worldwide efforts to marry the flexibility of organics with the functionality of more traditional inorganic materials, creating hybrid organic–inorganic structures having entirely new properties. These hybrid materials have taken the form of bulk, film, nanoparticles, and molecularly thin self-assembled monolayers (SAMs). SAMs have proven to be versatile in terms of the new properties they can bring to surfaces and interfaces. The applications are diverse: The on/off ratio of organic field effect transistors has been enhanced by 4 orders of magnitude by proper selection of a molecule that forms a SAM on the device electrodes and that templates the structure of the overlying organic semiconductor.¹ The dipole moments of SAM-forming molecules have been used to improve charge injection in organic Schottky diodes² and in model copper phthalocyanine/gold structures³ and to modify the work function of dielectrics such as BaTiO₃.⁴ A molecularly doped SAM on an organic light emitting diode (OLED) anode yielded a device with a 10⁴ increase in current density and luminescence relative to the device with a bare anode.⁵ SAMs patterned via microcontact printing have been used in conjunction with wet chemical etching in a low-cost method of fabricating display-related structures on films of transparent conducting oxides.⁶ Metal corrosion can be inhibited by monolayers of phosphonate SAMs.⁷ SAM-forming phosphonic acid molecules have been used as coadsorbates in dye-sensitized solar cells to improve

device efficiencies by the suppression of dark current.⁸ Mercaptosilane-based SAMs have been used to link CdS quantum dots to porous TiO₂ films for efficient quantum dot-sensitized solar cells.⁹ Many more examples can be found in the literature.

Although the thiol-based chemistry used to link various molecules to metals such as gold, silver, palladium, and platinum is fairly well understood, less is known about the numerous schemes used to attach organic molecules to oxide surfaces. Such surfaces appear frequently as transparent conducting layers in a variety of electronic devices that includes solar cells, electrochromic devices, organic light emitting diodes, and thin film transistors. Silanes, thiols,^{10–13} carboxylic acids, and phosphonic acids have all been used as molecular anchors on metal oxide surfaces.¹⁴ Silanes work well for some applications but have limitations due to a reliance on surface hydroxyl concentration (which can be much less than a monolayer on many metal oxides) and because of their tendency to hydrolyze and polymerize in solution.¹⁵ Phosphonic acids surmount many of these limitations.¹⁵ The application of thiol-based linking chemistry to metal oxides appears to be based somewhat on its historical use with gold surfaces where the strong Au–S bond (418 kJ/mol for the diatomic molecule)¹⁶ comes into play. Reported values for zinc–sulfur bonds range from 205 kJ/mol for the diatomic molecule¹⁶ to 430 kJ/mol for the Zn–S bond occurring between ethanethiol and aluminum-doped ZnO.¹⁷ This latter result from Rhodes and co-workers comes from application of density functional theory and stands apart from the well-studied *n*-alkanethiol-Au(111) system in which the desorption

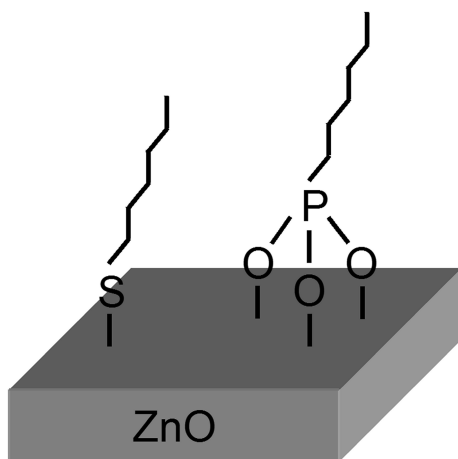


Figure 1. Schematic of the thiol and phosphonic acid-based SAMs.

enthalpy of the Au–S bond in a series of chemisorbed 2 to 14 carbon *n*-alkanethiols was consistently determined to be 126 kJ/mol.¹⁴

The strength of the bond between the anchor group and the surface is not the only factor determining the quality and functionality of a SAM. The two-sided nature of any linking group dictates that it will have an influence on the overall chemical stability of the molecule. In other words, the strength of the bond between the linking group and the rest of the molecule is also important, especially because many applications of SAMs involve processes conducted at elevated temperature. In this regard and for thiolates, a sulfur–carbon bond becomes important, whereas in phosphonic acids it is a phosphorus–carbon bond that is of interest (Figure 1). Consideration of bond lengths can yield insights into relative stability; however, in this case both the C–P bond and C–S bonds are approximately the same at 1.8 Å.^{18,19} Bond dissociation enthalpies are also similar: 73.6 kcal/mol²⁰ for the C–S bond in CH₃SCH₃ and ~65 kcal/mol for the four-coordinate C–P bond.²¹

This article provides a direct comparison between two of the more promising linking groups for ZnO, the thiol and phosphonic acid moieties. Our comparison of these anchor groups relies on the fact that SAM adsorption enthalpies can be partitioned into two components: that belonging to the alkyl group and that belonging to the anchor group.¹⁴ Use of identical *n*-hexyl analogues of each linking group ensured that the contributions by the alkyl chains to the total enthalpies of the molecule–substrate interactions were similar and that differences in the organic layers are due solely to the anchoring group. Our selection of a short hexyl group versus the much larger alkyl groups typically used in SAM formation stems from the realization that the electrical resistance of alkyl groups is exponentially dependent on the number of carbon atoms in the chain²² and the expectation that these results will be applicable to the tailoring of transport properties in next generation solar cells. In addition, for alkane chains shorter than ~octane, the chain–chain interactions are small relative to the anchor–group substrate interaction, and it is the latter that is the focus of the current work.¹⁴ For convenience, the term SAM is used to describe the short hexane-based monolayers despite the fact that organic portions of the thiol and phosphonic acid-based films are likely less well-ordered than those found in more typical SAMs formed from molecules with longer polymethylene chains. Although the anchor groups of even the shortest SAM-forming molecules can be highly ordered,^{23,24} the alkane portion of SAMs produced from both alkanethiols^{14,25} and alkane

phosphonic acids^{26–28} has been shown to be liquid-like at room temperature for chain lengths shorter than roughly 10 carbons.

Zinc oxide, an important material used widely in solar cells, catalysts, transducers, and elsewhere, was used as a substrate.²⁹ Although both thiol and phosphonic acid chemistries have been explored on other oxide surfaces, direct comparisons between the two as well as detailed information about both types of SAMs on ZnO are limited in the literature, in particular for phosphonic acid SAMs. Taratula et al. compared among other molecules the binding of *n*-hexanethiol and phenylphosphonic acid on ZnO films and nanorods.¹³ Their IR and UV–vis absorbance data indicated that neither molecule chemisorbed significantly on ZnO. Brewer et al. conducted an experimental and theoretical comparison of C-8, C-12, and C-16 alkanethiolate and dodecanephosphonate (C-12) monolayers on indium–tin oxide (ITO).³⁰ Among their findings were density functional theoretical results indicating that the bond enthalpy of phosphonate to either indium or tin was less than that of the corresponding thiolate. This calculation stands in contrast to earlier experimental work in which it was found that ITO, when exposed to a solution containing equal concentrations of structurally similar phosphonic acid and thiol molecules, selectively adsorbed the phosphonic acid in a ratio of ~100:1.³¹

The work reported here revisits the topic of thiol versus phosphonic acid anchor groups and provides guidance for the attachment of molecules to an important transparent conducting oxide. We have not attempted to elucidate fully the bonding configuration of hexanephosphonic acid and hexanethiol on ZnO; such a detailed description is beyond the scope of the current work. Instead, the emphasis is on a relative comparison of the two anchor groups. A combination of angle-resolved photoelectron spectroscopy, temperature-dependent photoelectron spectra, contact-angle measurements, and data from a novel QCM-based flow reactor was used for this purpose. The results form a consistent picture of the relative merits of the thiol and phosphonic acid linking groups as well as shed light on previous claims^{11,12,17} of highly stable alkanethiolate monolayers on ZnO.

Experimental Methods

QCM-Flow Reactor. Our interest in solid–liquid interfaces led to the construction of the home-built QCM-based flow reactor described briefly in a previous publication.³² Figure 2 is a schematic of our setup. The apparatus allows the automated flow of liquid reagents across the front surface of a QCM oscillator. Polished, SiO₂-coated QCM crystals were sputter-coated with a 500 nm layer of undoped ZnO using a relatively low growth temperature of 200 °C to keep film roughness to a minimum. Except for the pumps and electronics, components are located inside the glovebox portion of a cluster tool comprised of electron spectroscopy systems, a physical vapor deposition chamber, and an 8 m long ultrahigh vacuum (UHV) transport system that links the other components. Thus, films either grown or etched in the flow reactor can be transferred without air exposure to analytical or deposition stations for further work. Wetted materials of the flow reactor are comprised of fluoropolymer or polypropylene with the exception of the stainless steel inlet and outlet of the flow cell, and of some epoxy potting in the membrane contactors.³³ The latter are devices that allow the removal or addition of gases to the reagent streams. Solutions of reagents can be transported to the flow cell³⁴ either by computer controlled peristaltic reagent pumps³⁵ or by gravity. Ammonium chloride has been shown to be an effective and controllable etchant for ZnO³⁶ and in the QCM-flow reactor

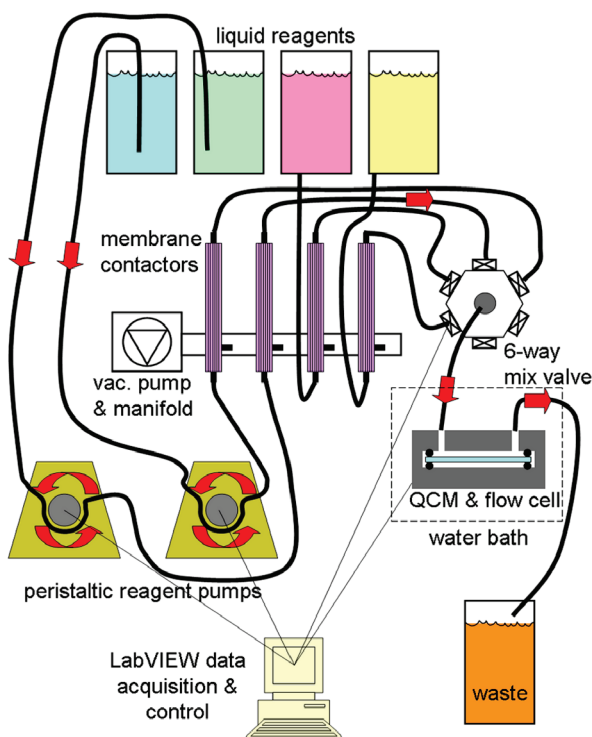


Figure 2. Schematic of our QCM-based flow cell reactor used to probe the quality of SAMs.

experiments a 5 mM solution in 95% ethanol was used as a probe of SAM quality. The crystal resonance frequency was monitored with a commercial crystal monitor³⁷ and converted to thickness within *LabVIEW* using the following relation developed by Lu and Lewis:³⁷

$$\Delta m = \left(\frac{N_q \rho_q}{\pi R_z f} \right) \tan^{-1} \left[R_z \tan \left[\pi \left(\frac{f_q - f}{f} \right) \right] \right] \quad (1)$$

where Δm is the thickness in g/cm², N_q is a frequency constant for the crystal, ρ_q is the density of quartz, R_z is the Z-factor or ratio of the acoustic impedances of quartz and the film material, f_q is the frequency of the unloaded crystal, and f is the frequency of the loaded crystal. Switching between different fluids was accomplished using a six-inlet, one-outlet solenoid controlled mixing valve.³⁸ When switching from one reagent to another, a purge of pure solvent (95% ethanol) was used to eliminate bulk mixing of different reagents. Initial results from the system indicated that the quartz crystal resonant frequency changed slightly as a result of small temperature fluctuations in the reagent streams caused by power dissipation in the mixing valve solenoids. Installation of a “hit and hold” circuit³⁹ that reduced within 0.1 s the voltage applied to the solenoid to one-third of its initial value greatly reduced these temperature-induced artifacts. Data acquisition and control of the entire apparatus was performed using *LabVIEW*-based software and hardware from National Instruments.

Growth of SAMs. *N*-hexylphosphonic acid (HPA) was purchased from STREM chemicals and used without further purification. *N*-hexanethiol and ammonium chloride were purchased from Sigma-Aldrich and used without further purification. Solutions of the thiol and phosphonic acid (2 mM in 95% ethanol) were prepared and used in a glovebox free of molecular oxygen; in the case of the thiol this helps prevent formation of the corresponding disulfide.⁴⁰ Polycrystalline ZnO substrates

were cleaned with acetone, ethanol, and UV/O₃ cleaning for 15 min and were found to be clean when examined by XPS. Single-crystal ZnO substrates were cleaned within the photoemission system with 20 min of 1 kV argon ion sputtering ($\sim 10 \mu\text{A}/\text{cm}^2$), followed by annealing to 450 °C in UHV. Cleaned substrates were exposed to the thiol and phosphonic acid solutions for the specified time, rinsed thoroughly with 95% ethanol, blown dry with nitrogen, and transferred to the photoemission chamber for analysis. As has been observed previously on SiO₂⁴¹ and ITO⁵ films, a basic potassium carbonate wash was found to remove phosphonic acid-derived SAMs that had not been annealed to ~ 150 °C and not to remove those that had (data not shown). Because our QCM experiments were conducted under acid conditions and because our room-temperature XPS and contact angle results were not affected by annealing, this procedure was not performed for the phosphonic acid SAMs investigated here.

XPS Analysis. Angle-resolved and temperature-dependent X-ray photoelectron spectroscopy measurements were performed using a modified PHI 5600 photoemission system that has been described previously.⁴² The system uses sample holders equipped with electrical connections for a thermocouple, thereby allowing direct attachment of a thermocouple to the sample. For temperature-dependent work XPS, a third type of substrate was prepared that consisted of undoped polycrystalline ZnO sputter deposited on 0.010" Mo foil at 200 °C. A type-K thermocouple was spot-welded to a 4 mm² piece of tantalum foil that was then pressed firmly to the top of the ZnO/Mo film. Samples were heated in UHV indirectly with a resistive heating element; temperature was controlled with a Eurotherm 2204e controller. Temperature-dependent XPS spectra were taken with a pass energy of 29.4 eV, slit #4, and the instrument set up with the angle-integrating minimum area mode that corresponds to an acceptance angle of $\pm 7^\circ$. The takeoff angle for the temperature-dependent measurements was 45°. Monochromatic Al K α radiation was used for all experiments.

Angle-resolved substrate attenuation data were taken with a pass energy of 29.4 eV using slit #4 and the large area mode of our instrument that corresponds to an acceptance angle of $\pm 2^\circ$. SAM thicknesses were calculated from angle-resolved XPS spectra using the inelastic-mean-free-path of 31 Å for *n*-paraffin taken from the NIST database⁴³ and standard intensity-angle relationships.⁴⁴ In all cases, the Zn 2p_{3/2}, O 1s, C 1s, P 2s, and S 2p regions were examined over a 20 eV range in 0.125 eV increments and using acquisition time/data point values of 0.5 s, 1.0 s, 2.5 s, 5.0 s, and 5.0 s, respectively. Care was taken to examine a different portion of each sample at every angle to avoid X-ray induced damage to the organic layer.

Peak fitting was performed using a Shirley background and the sum version of the Voigt approximation.⁴⁵ For transitions (e.g., O 1s) showing more than one chemical component, the primary component was not fixed in energy because of the changes in band bending that are known to occur in ZnO as a result of changing surface chemistry.⁴⁶ Unless noted, the peak positions of other chemical components were fixed in energy relative to the primary component, and peak full-width-at-half-maxima (FWHMs) and Gaussian–Lorentzian mixing for a given transition were constrained to be the same. The spin–orbit splitting of the S 2p_{1/2} and 2p_{3/2} peaks was constrained to 1.18 eV⁴⁷ and an area ratio of 1:2.⁴⁸

Contact Angle Measurements. Sessile drop contact angles were measured with deionized water and in air using a Krüss DSA100 drop shape analysis system. Drops of 1 μL were used. For these experiments, a fourth type of sample consisting of

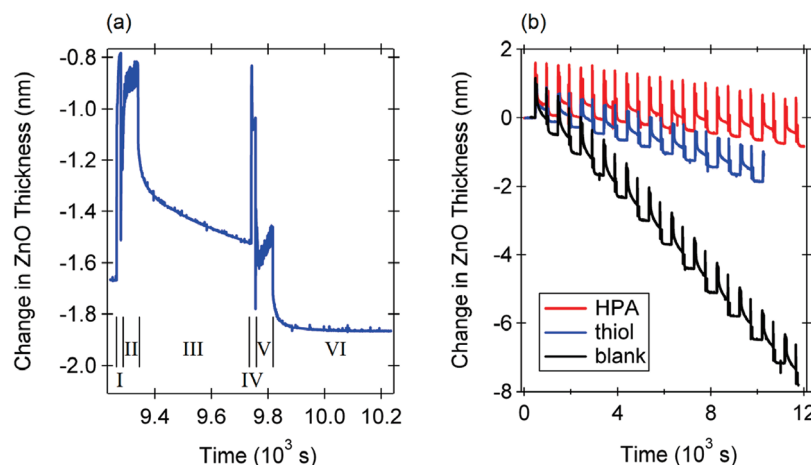


Figure 3. Output from the QCM-flow reactor. Panel (a) is small portion of the data in panel (b) and shows the fluid injection sequences *I*–*VI* that correspond to one full cycle. Panel (b) shows traces for the *n*-hexanephosphonic acid SAM (red), the *n*-hexanethiol–SAM (blue), and the control case of no SAM formation with ethanol (black).

aluminum-doped ZnO on glass⁴⁹ was used because of its flatness. Contact angles were measured from videos taken starting 10 s after drop deposition, yielding 32 contact angles per run. Three runs were performed for each SAM and results were averaged for the reported contact angles.

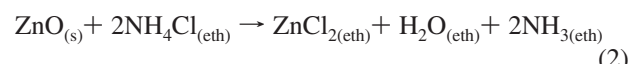
Results and Discussion

QCM-Flow Reactor. Figure 3 is comprised of data from our QCM-flow reactor. Panel a is an expanded plot of data in panel b and shows a typical pulse sequence used to probe the relative quality of SAMs on ZnO. *Region I* of part a of Figure 3 corresponds to a gravity-fed purge of the flow cell for 15 s using clean 95% ethanol. A decrease in the crystal frequency due to the changing fluid pressure during the purge is registered as an anomalous positive change in film thickness of about 0.9 nm. Injection via peristaltic pump of the 5 mM ammonium chloride solution takes place over a 60 s period in *region II*. In the 400 s long *region III*, there is no flow across the QCM sensor, and the SAM/ZnO structure is being etched by the ammonium chloride solution. Another gravity-fed 15 s purge of the flow cell takes place in *region IV*. *Region V* corresponds to the pump injection of a solution of the SAM-forming molecule, *n*-hexanethiol in this case. In *region VI*, the flow cell and QCM sensor are again in a static, no-flow condition while the SAM-forming molecules self-assemble for 420 s on the ZnO surface. For each molecule tested as well as the ethanol blank, the entire *I*–*VI* sequence repeats about 10–12 times during which time $\sim 2 \times 10^5$ thickness readings are taken.

A representative data set from the flow reactor is shown in part b of Figure 3. The only difference among the three runs is the composition of the solution in the previously described *region V*, injection of the solution of the SAM-forming molecule. For the black trace labeled “blank”, *region V* was simply the 95% ethanol solvent used to make the HPA and *n*-hexanethiol solutions. The overall ZnO etch rate for this blank run was 0.016 Å/s. Injecting an *n*-hexanethiol solution in *region V* resulted in the formation of SAM that reduced the ZnO etch rate to 0.0047 Å/s. The lowest etch rate was found after exposure of the ZnO to HPA solution and was 0.0017 Å/s.

Our QCM-based flow-reactor results can be viewed as an electroless version of experiments in which the electrical conductivity and ionic permeability of self-assembled mono-

layers are probed electrochemically.⁵⁰ In the case of unprotected ZnO and in the presence of the Brønsted acid ammonium chloride, corrosion takes place according to the following:



Here, the (eth) subscript denotes an ethanolic solution. In the case of ZnO protected by a self-assembled monolayer of hydrophobic *n*-hexyl groups, approach of the hydrophilic ammonium and hydronium ions to the ZnO surface is inhibited and the etch rate is reduced. Thus, the data in Figure 3 demonstrate that the phosphonic acid group produces SAMs that are more uniform and possibly more compact than ones produced using a thiol anchor group, at least on the 420 s time scale used in our flow reactor experiments for SAM formation. Although this time scale is relatively short, previous work has shown that longer C-18 alkanethiols can form well-ordered SAMs on ZnO within 300 s followed by slow conformational ordering that takes place over a period of hours or days.⁵¹ The 420 s time period used in our flow cell measurements was chosen as a balance between the formation of compact, high coverage monolayers and the time needed to perform 10–12 complete fluid injection cycles.

Angle-Resolved XPS. SAMs were prepared on ZnO(0001)-O single crystals for angle-resolved XPS measurements. For both HPA and *n*-hexanethiol, longer adsorption times of 20 min and 16 h were used to improve ordering of the alkyl chains and increase overall SAM coverage. Figure 4 shows the carbon/phosphorus and carbon/sulfur atomic ratios as a function of electron takeoff angle for SAMs formed from the two molecules during the two time periods. For these data a takeoff angle of 90° corresponds to the electrons’ exit along the surface normal. The $\sim 40\%$ increase in the carbon to anchor group ratio with decreasing exit angle implies that both the HPA and *n*-hexanethiol molecules adsorbed with the head–tail orientation depicted in Figure 1, with their alkyl chains away from the surface and the anchor group attached to the surface. The fact that the carbon to sulfur ratio of the thiol–SAM formed during 20 min is much higher than the expected value of six indicates that in this SAM some of the C 1s signal had a source other than the parent thiol molecule. This high and nonstoichiometric carbon–sulfur ratio is not surprising given that for these short

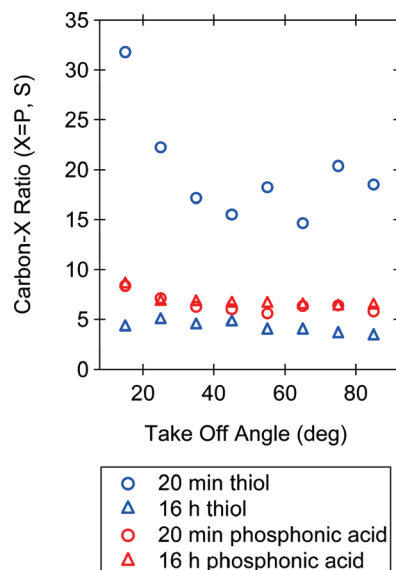


Figure 4. Angle-resolved XPS measurements showing the atomic ratios of carbon to either phosphorus or sulfur as a function of takeoff angle and for different immersion times in the SAM solutions. A takeoff angle of 90° corresponds to electrons exiting along the surface normal.

TABLE 1: Immersion Times and XPS-Derived Thickness of SAMs Formed on ZnO(0001)-O by *n*-Hexanethiol and *n*-Hexanephosphonic Acid^a

immersion time	SAM thicknesses (Å)	
	<i>n</i> -hexanethiol	<i>n</i> -hexanephosphonic acid
20 min	2.5 ± 0.3	6.1 ± 0.4
16 h	3.3 ± 0.4	5.8 ± 0.6

^a The uncertainties are 95% confidence intervals.

adsorption times the absolute sulfur concentration is low (<1%) and that some carbon signal inevitably stems from the ethanol solvent and associated impurities. Slow adsorption of the thiol is indicated by the change in the carbon/sulfur ratio that occurs between 20 min and 16 h. In contrast, the HPA molecule is seen to form SAMs with essentially the same carbon/phosphorus ratio at short adsorption times as at longer adsorption times.

From the attenuation of the Zn 2p_{3/2} and O 1s photoelectron lines of the substrate by the molecular overlayers, it is possible to extract thicknesses of the SAMs for each takeoff angle. Results are given in Table 1. The XPS-calculated thickness of the HPA SAM were ~6 Å, shorter than expected from the gas-phase length of the HPA molecules (10.7 Å)⁵² but in reasonable agreement to that found experimentally. Love et al.⁵³ found that SAMs of *n*-alkanethiols on palladium had thicknesses $T = 1.87$ (Å/carbon atom) – 7.7 Å, which translates to only 3.5 Å for hexanethiol. Slightly thicker films were found on gold. The corresponding adsorbed phosphonic acid should be longer by approximately one P–O bond (1.6 Å),²¹ yielding an expected thickness of 5.1 Å for the HPA SAMs formed here. Wong and co-workers⁵⁴ found that alkyl monolayers covalently attached to silicon had lengths $L = 1.26$ Å/carbon – 0.7 Å, which yields an expectation of 8.3 Å for a HPA monolayer. Discrepancies among these values have been attributed to differences in tilt angle as well as the poorly characterized increasing degree of disorder found in short alkyl chains. Nevertheless, the fact that the SAMs formed on ZnO by *n*-hexanethiol are thinner than those formed by HPA even after accounting for the longer length of the phosphonic acid anchor group implies that the latter yields

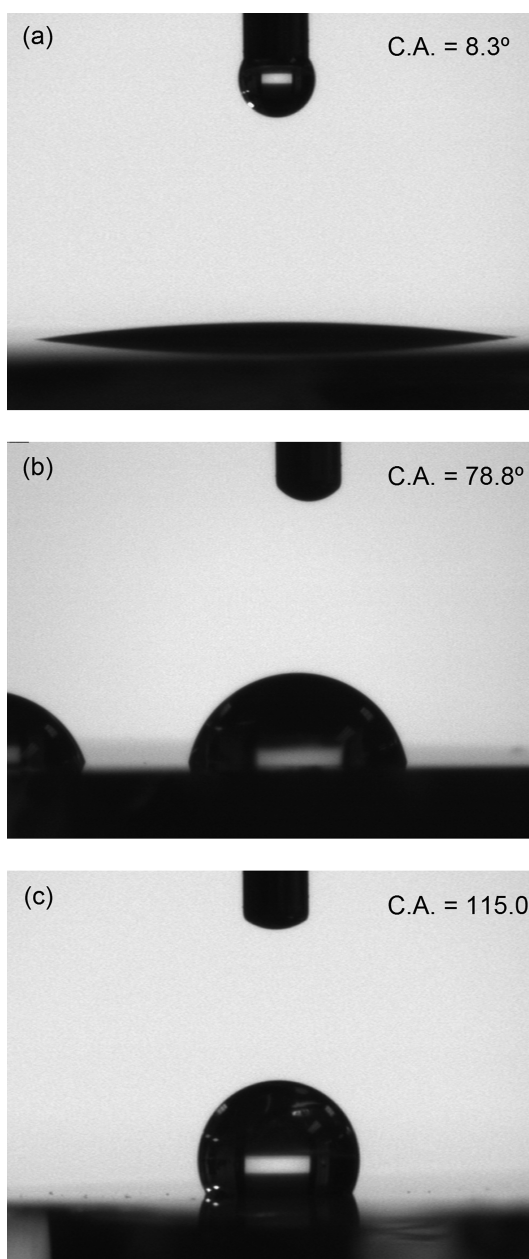


Figure 5. Photographs from water contact angle measurements on (a) ZnO cleaned with UV/O₃ and ethanol (b) *n*-hexanethiol-treated ZnO and (c) *n*-hexanephosphonic acid-treated ZnO.

more compact and uniform films, consistent with the QCM-flow reactor results.

Contact Angles. Sessile drop contact angle measurements were performed to ascertain the quality of hexyl monolayers formed by the two anchor groups. The longer exposure time of 16 h was used and results are shown in Figure 5. Panel (a) is a control and shows a 1 μL water droplet on a ZnO film that was first cleaned with UV/O₃ and then washed with ethanol. Ethanol washing was performed to make sure that this process, used in all SAM preparations, was not leaving a residue that could affect contact angle determinations. The average contact angle for the UV/O₃/ethanol-cleaned film was 8.3°. Panel (b) shows that exposure of the UV/O₃-cleaned film to *n*-hexanethiol for 16 h increased the hydrophobicity of the surface, yielding an average contact angle of 78.8°. The largest contact angle was found for the HPA-functionalized surface and was 115.0°. This latter result compares extremely well with contact angles of 101° and 118° found for octadecyltrichlorosilane⁵⁵ and stearic acid-function-

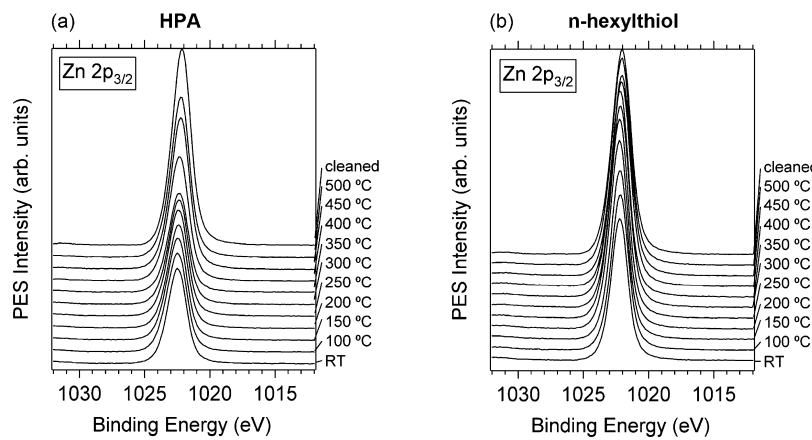


Figure 6. XPS spectra of the Zn 2p_{3/2} region for SAMs annealed to different temperatures in UHV. Panel (a) is the HPA SAM and panel (b) is the thiol-SAM.

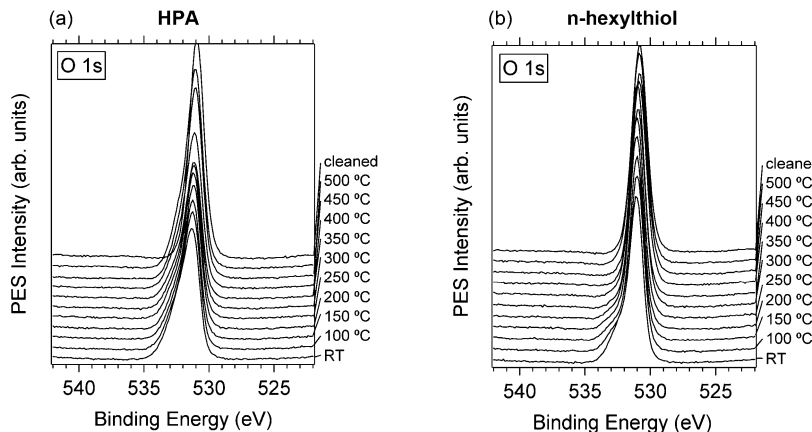


Figure 7. XPS spectra of the O 1s region for SAMs annealed to different temperatures in UHV. Panel (a) is the HPA-SAM and panel (b) is the thiol-SAM.

alized⁵⁶ ZnO surfaces, especially so because of the use of much longer alkane chains in the case of refs 55 and 56. The larger contact angles found using HPA versus *n*-hexanethiol are consistent with the flow reactor and XPS-thickness results showing a more uniform and more hydrophobic hexyl monolayer formed using the phosphonic acid anchor group than with the thiol anchor group.

Temperature-Dependent XPS. SAMs of both *n*-hexanethiol and HPA were prepared on 500 nm thick ZnO film sputter-grown on molybdenum foil. X-ray photoelectron spectra were taken on as-grown films (labeled RT for room temperature), and films heated in UHV from 100 to 500 °C in 50° increments. One additional spectrum for each core level labeled clean corresponds to the ZnO film after argon ion sputtering and annealing in UHV to 450 °C. Results for the Zn 2p_{3/2} region are shown in Figure 6. For both films, a single component appears in the as-deposited film around 1022.1 eV and in the case of the HPA SAM, shifts by 0.4 eV to higher binding energy with increasing temperature. The Zn 2p_{3/2} peak from the thiol-modified film increases in binding energy only slightly (0.1 eV) with increasing annealing temperature. The lower intensity of the Zn 2p_{3/2} peak for the HPA-functionalized surface relative to the *n*-hexanethiol-functionalized surface is consistent with the higher HPA-SAM coverage indicated in Table 1.

Figure 7 shows O 1s spectra for the HPA and *n*-hexanethiol-SAMs. Both as-grown SAM/ZnO structures show a main O 1s peak at 531.2 eV and with a 1.2 eV FWHM originating from the ZnO lattice. Because of changes in band bending occurring during annealing, additional O 1s components

seen at higher binding energy are given relative to the lattice oxygen peak. An additional peak observed in both SAMs at 1.9 eV higher than the lattice oxygen peak is attributed to -OH based on previous work⁵⁷ and its decrease with increasing annealing temperature. The series of HPA-SAM O 1s spectra were best fit with a third peak located at 1.0 eV above that belonging to the lattice oxygen. This was ascribed to P-O-Zn bonding.⁵⁸ A third peak was also used to fit the *n*-hexanethiol-SAM O 1s spectra and was located at 0.9 to 1.1 eV above the lattice oxygen peak. The chemical species associated with this peak is not clear at this point but the S 2p spectra discussed below point toward S-O bonding. Fixing the position of this peak relative to the lattice oxygen peak during the fitting procedure as was done for the HPA-SAM data resulted in a decrease of fit quality, an indication of changing chemical composition. Finally, it can be seen that with increasing temperature, the overall O 1s line-shape for the HPA-SAM changes little, and that the higher BE components in the *n*-hexanethiol-SAM O 1s spectra are removed.

Determination of the hexanephosphonic acid bonding configuration in the SAM necessitated that a reference spectrum of bulk HPA be obtained for comparison. A thick film of pure HPA was produced on a clean Si wafer by drop-casting from an ethanol-water solution (0.3 g/50 mL). Only carbon, oxygen, and phosphorus were detected in a wide-range survey spectrum (data not shown). Atomic ratios for carbon, oxygen, and phosphorus using literature sensitivity factors were 5.3:2.6:1, close to the values expected from stoichiometry. Figure 8 shows O 1s, C 1s, and P 2s spectra from a HPA-SAM and from the

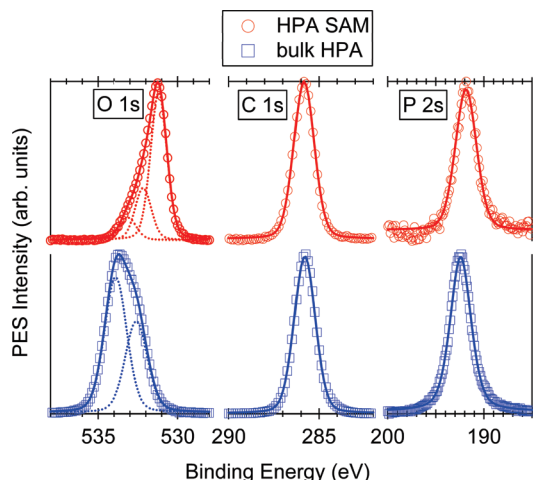


Figure 8. XPS spectra of the O 1s, C 1s, and P 2s regions of the HPA-SAM (top, red circles) and of a thick, bulklike film of HPA (bottom, blue squares) produced by drop-casting. Data are indicated with markers, fitted components with dotted lines, and the overall fit with solid lines.

bulk film of HPA. The insulating nature of the drop-cast HPA film resulted in the film charging during analysis; a low intensity and low-energy electron beam was used for charge neutralization. For comparison, the binding energy scales of the drop-cast film and the SAM were aligned using the C 1s peak of the SAM at 285.9 eV. The O 1s spectrum of the drop-cast film has two components appearing at 533.9 and 532.6 eV and with an area ratio of 60:40. On the basis of the relative areas, the 533.9 eV peak was assigned to the two $-\text{OH}$ groups of the phosphonic acid and the 532.6 eV peak to the phosphoryl oxygen ($\text{P}=\text{O}$). The difference between these components (1.3 eV) is similar to that observed by Adolphi et al. (1.5 eV)⁵⁸ and Textor et al. (1.5 eV)⁵⁹ but substantially smaller than the 3.3 eV value reported by Hanson and co-workers.⁵ Interestingly, neither bulk phosphonic acid component appears in the O 1s spectrum of the HPA-SAM. Because of this and because only a single component of the SAM O 1s spectrum was found to be associated with phosphorus, it is likely that the primary form of hexanephosphonic acid chemisorbed on ZnO is a tridentate phosphonate as depicted in Figure 1 and been found for adsorption on other metal oxides.^{5,60,61} Note that the shift by 0.5 eV of the P 2s peak to lower binding energy that occurs with chemisorption is consistent with this picture and with the loss of the multiple bonds between oxygen and phosphorus that exist within the phosphoryl group of the bulk HPA.

Figure 9 is comprised of the phosphorus 2s spectra from the UHV-annealed HPA-SAM and the sulfur 2p spectra from the *n*-hexanethiol-SAM. In Panel (a) the P 2s spectrum of the cleaned ZnO film shows two small peaks from chlorine at ~ 200 eV that are removed by exposure of the film to the HPA solution. The peaks shapes, intensities, and positions of the P 2s transition in the HPA-SAM data are essentially constant and centered on 191.7 eV with increasing temperature. In contrast, chemical changes occurring in the thiol-based SAM are reflected in the S 2p spectra in part b of Figure 9. Starting at 200 °C, the S $2p_{3/2}$ component shifts to lower binding energy from its initial position at 163.1 eV. A previous XPS and temperature programmed desorption (TPD) study of methanethiol on ZnO has demonstrated that this S $2p_{3/2}$ binding energy is indicative of thiolate bound to zinc sites.⁶² The low-intensity broad peak centered on 169 eV is assigned to a small amount of S–O bonding and is seen to disappear by 350 °C.⁴⁷ The presence of partially oxidized hexanethiol on ZnO could

mean either that there was some amount of contamination from oxygen-containing reagents or that a small percentage of the adsorbed thiol molecules were able to react with the oxygen sublattice. The latter is likely, given the numerous step and kink defects available to the hexanethiol molecules on the polycrystalline films used for the temperature-dependent XPS experiments and given that the SAMs were prepared and analyzed without exposure to air. At 500 °C, the intensity of the main S 2p peak at 162.5 eV, assigned to atomic S bound to Zn,⁶² starts to disappear. It should be noted that the hump in the S 2p data centered on ~ 158 eV is a plasmon loss from the Zn 3s transition and is not related to sulfur.

Spectra from the C 1s region are shown in Figure 10. For the phosphonic acid SAM, the single-component aliphatic C 1s peak at 285.9 eV has a constant intensity up to 350 °C in the series of spectra in part a of Figure 10. The C 1s peak from the *n*-hexanethiol-SAM is seen in part b of Figure 10 to decrease in intensity slightly with the first anneal to 100 °C and to have negligible intensity after the sample has been heated to 400 °C. Neither film yielded extra C 1s components due to differential charging, an indication of an absence of multilayers.⁶³ For both SAMs, changes in the C 1s binding energy at higher temperatures indicate decomposition of the SAM-forming molecule.

The results from Figures 6, 7, 9, and 10 are summarized in Figure 11. Panel (a) shows the absolute surface concentration of the two anchor groups as a function of temperature. Both sulfur and phosphorus appear to be quite stable on the ZnO surface, remaining to the point where some sublimation of the ZnO itself is expected to take place.⁶⁴ Panel (b), a plot of the carbon to anchor group ratio as a function of temperature, tells a different story about the stability of the molecular layers. Assuming no gross molecular decomposition upon adsorption, both SAMs should start out with a 6:1 ratio of carbon to anchor group; small deviations from this can be attributed to our use of literature sensitivity factors and the fact that the molecules are oriented with their alkyl chains extending out into the vacuum. Still, it is clear that the *n*-hexanethiol-SAM is quite fragile thermally and begins to degrade at a temperature of less than 100 °C. In contrast, part b of Figure 11 shows that the stoichiometry of the HPA-SAM is preserved up to 350 °C and implies that even at that high temperature the essence of the HPA molecular structure is retained.

Our conclusion that alkanethiol-derived SAMs on ZnO are thermally fragile is at odds with several recent studies. Sadik et al. showed results for the thermal stability of dodecanethiol adsorbed on the zinc and oxygen terminated faces of $\langle 0001 \rangle$ -oriented ZnO single crystals, claiming that the thiol was stable on the Zn-terminated surface up to about 400 °C and to 350 °C on the O-terminated surface.¹² Ogata and co-workers claimed that propanethiol was stable on ZnO(0001)-O up to 400 °C.¹¹ Rhodes et al. focused the theoretical portion of their study on the zinc–sulfur bond and concluded partially on the basis of a calculated large Zn–S bond enthalpy that their C_{16} and C_{18} -thiolate monolayers on aluminum-doped ZnO were robust.¹⁷ In all of these studies, the authors focused on the sulfur–zinc oxide interaction, neglecting the other side of the molecular anchoring group. In refs 11 and 12, the intensity of the S 2p core level was followed and used as the sole measure of the thiol coverage in temperature-dependent measurements. Unfortunately, neither group published C 1s data along with their S 2p spectra. This would have been useful because our results indicate C–S bond scission occurs at quite low temperatures in the *n*-hexanethiol–ZnO system. This is consistent with previous

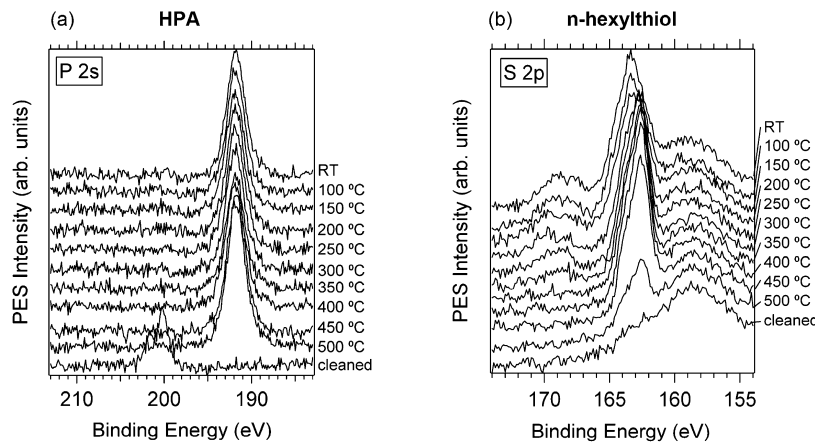


Figure 9. XPS spectra for SAMs annealed to different temperatures in UHV. Panel (a) is the P 2s region of the HPA SAM and panel (b) is the S 2p region of the thiol-SAM.

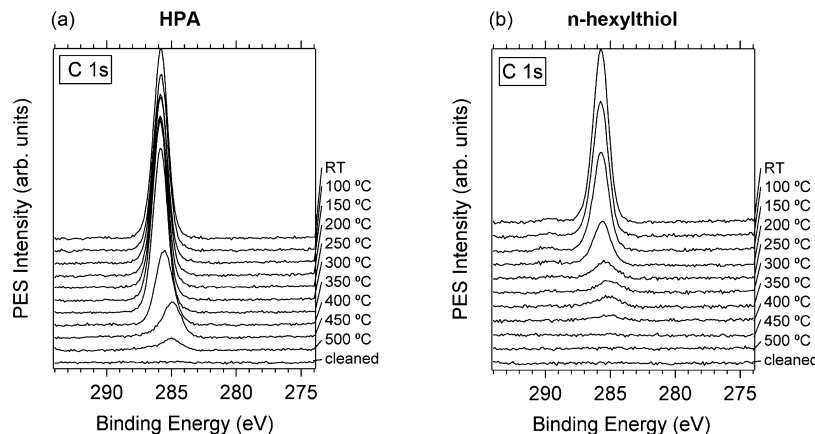


Figure 10. XPS spectra of the C 1s region for SAMs annealed to different temperatures in UHV. Panel (a) is the HPA SAM and panel (b) is the thiol-SAM.

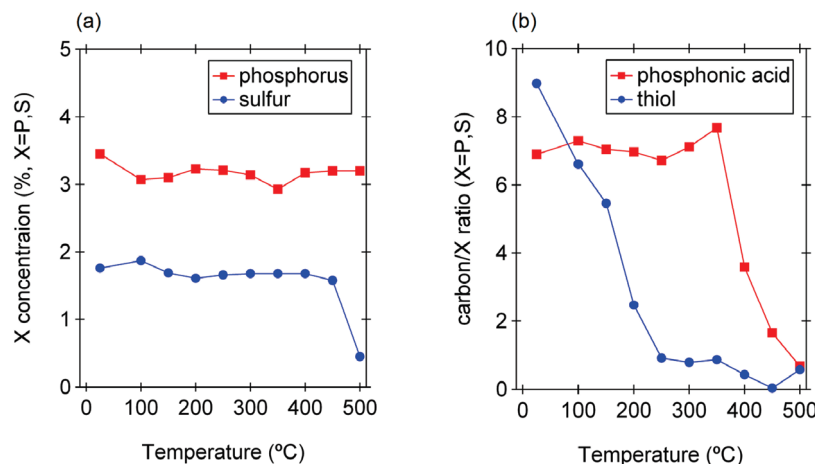


Figure 11. In panel (a), the absolute surface concentration of sulfur and phosphorus in SAMs annealed to different temperatures in UHV. In panel (b), the ratio of carbon to either phosphorous or sulfur in the SAMs as a function of temperature.

TPD and photoemission results for methanethiol⁶² and ethanethiol⁶⁴ adsorbed on ZnO that demonstrated C–S bond scission at 227 and 187 °C, respectively. These studies demonstrated that, following thiolate decomposition, sulfur atoms remained on the surface until \sim 557 °C, at which point they desorbed as SO₂. Clearly, the amount of sulfur by itself is a poor measure of the presence of intact alkanethiolate molecules on ZnO. Thus, although our temperature-dependent sulfur photoemission data are consistent with these previous reports,^{11,12} our conclusions about the stability and utility of the thiol linking group are not.

One could argue that alkanethiols with chains longer or shorter than hexanethiol might have dramatically better thermal stability, but this view is not borne out by the literature. A TPD and XPS study of alkanethiols on Cu(110) indicated that carbon–sulfur bond scission in CH₃(CH₂)₃SH and CH₃(CH₂)₂SH began at -3 °C and at lower temperatures than CH₃SH.⁶⁵ These same techniques were used to probe the thermal reactions of alkanethiols on GaAs(100) and showed that the most stable thiolate adsorbate on an As site undergoes carbon–sulfur bond cleavage at 247 °C independent of alkyl chain length.⁶⁶ Shih

and co-workers used TPD and IR spectroscopy to study the thermal reactions of mercaptoethanol on clean and oxygen-precovered Cu(100) and concluded that C–S bond scission began at ~ 42 °C.⁶⁷ The C–S bond in *n*-decanethiol adsorbed on copper was observed to have low thermal stability, cleaving at ~ 100 °C.⁶⁸ For alkanethiol monolayers on gold and in contact with hexadecane, ellipsometry results demonstrated that longer alkyl chains lead to greater thermal stability, but desorption still occurred at quite low temperatures (>70 °C).²⁵

TPD results for alkylphosphonates on metal oxides have not been reported in the literature, however thermogravimetric analyses of bulk zinc phosphonates yield insights into the thermal stability of our hexanephosphonate-ZnO system. Menaa et al. showed that zinc vinylphosphonate was stable up to 560 °C in flowing nitrogen.⁶⁹ Zinc propylenebis(phosphonates) were found to lose their organic groups at ~ 520 °C.⁷⁰ Removal of the phenyl ring from zinc phenylphosphonate was found to occur at >500 °C.⁷¹ For comparison, similar bulk zinc alkanethiolates typically decompose at <250 °C.^{72,73}

Conclusions

We have compared the efficacy of the thiol and phosphonic acid linking groups for ZnO by studying SAMs prepared from *n*-hexane derivatives of both. We report the development of a novel QCM-based flow reactor and a method to use a dilute acid as a probe of the quality of SAMs on ZnO. Data from the QCM-flow reactor demonstrate that both *n*-hexanethiol and HPA provide significant corrosion protection for ZnO in contact with the Brønsted acid ammonium chloride, with HPA being more effective than *n*-hexanethiol. Water contact angle determinations confirmed QCM-flow reactor results and indicated that SAMs produced using HPA were more hydrophobic than those prepared using *n*-hexanethiol. Angle-resolved XPS results showed that both molecules adsorbed with their anchor groups pointing toward the ZnO surface and alkyl chains pointing away from the surface. Analysis of the attenuation of signals from the ZnO substrate by the molecular overlayers enabled quantification of the thicknesses of SAMs formed from the two molecules: HPA-derived SAMs were found to be ~ 6 Å thick, about twice as thick as those formed from *n*-hexanethiol. Stoichiometric SAMs formed from HPA within 20 min; the carbon/sulfur ratio of *n*-hexanethiol-derived SAMs was much larger than the expected value of six for short exposures and decreased over time, indicating slower adsorption for *n*-hexanethiol than for HPA. Temperature-dependent XPS spectra of the C 1s region contradict recent reports of stable alkanethiolate monolayers on ZnO and showed that C–S bond scission occurs at relatively low temperatures in these systems, in contrast to the HPA SAMs, which remained intact to 350 °C.

The work presented here provides guidance for attachment of molecules to the important transparent conductor ZnO. Even the relatively short alkyl groups used here could possibly serve as corrosion inhibitors in ZnO-based TCOs used in solar cells, an application in which the oxide is frequently exposed to acids that are decomposition products of acetate encapsulants.⁷⁴ In addition, the intrinsic thermal instability of hexanethiol on ZnO implies that impressive increases observed in the performance of devices utilizing similar SAMs might have an origin more complex than currently thought, especially for devices that have undergone processing at elevated temperatures.^{1,10,75,76} Finally, although these results indicate that for alkyl chains on ZnO the phosphonic acid moiety functions as a superior linking group than does thiol, SAM applications in which electrical transport

is important, for example dye monolayers in sensitized solar cells may benefit from the choice of a different molecular anchor.

Acknowledgment. The author would like to thank Xiaonan Li for growth of the ZnO films used in QCM and temperature-dependent XPS experiments, Chun-Sheng Jiang for AFM measurements, and Sheyu Guo from EPV Solar for the ZnO:Al/glass films. This work was supported by the U.S. Department of Energy under Contract No. DE-AC36-08-GO28308 with the National Renewable Energy Laboratory.

References and Notes

- Bock, C.; Pham, D. V.; Kunze, U.; Kafer, D.; Witte, G.; Woll, C. Improved morphology and charge carrier injection in pentacene field-effect transistors with thiol-treated electrodes. *J. Appl. Phys.* **2006**, *100* (11), 114517.
- Campbell, I. H.; Kress, J. D.; Martin, R. L.; Smith, D. L.; Barashkov, N. N.; Ferraris, J. P. Controlling charge injection in organic electronic devices using self-assembled monolayers. *Appl. Phys. Lett.* **1997**, *71* (24), 3528–3530.
- Chen, W.; Huang, C.; Gao, X. Y.; Wang, L.; Zhen, C. G.; Qi, D. C.; Chen, S.; Zhang, H. L.; Loh, K. P.; Chen, Z. K.; Wee, A. T. S. Tuning the hole injection barrier at the organic/metal interface with self-assembled functionalized aromatic thiols. *J. Phys. Chem. B* **2006**, *110* (51), 26075–26080.
- Schulmeyer, T.; Paniagua, S. A.; Veneman, P. A.; Jones, S. C.; Hotchkiss, P. J.; Mudalige, A.; Pemberton, J. E.; Marder, S. R.; Armstrong, N. R. Modification of BaTiO₃ thin films: adjustment of the effective surface work function. *J. Mater. Chem.* **2007**, *17* (43), 4563–4570.
- Hanson, E. L.; Guo, J.; Koch, N.; Schwartz, J.; Bernasek, S. L. Advanced surface modification of indium tin oxide for improved charge injection in organic devices. *J. Am. Chem. Soc.* **2005**, *127* (28), 10058–10062.
- Breen, T. L.; Fryer, P. M.; Nunes, R. W.; Rothwell, M. E. Patterning indium tin oxide and indium zinc oxide using microcontact printing and wet etching. *Langmuir* **2002**, *18* (1), 194–197.
- Amar, H.; Benzakour, J.; Derja, A.; Villemain, D.; Moreau, B.; Braisaz, T. Piperidin-1-yl-phosphonic acid and (4-phosphono-piperazin-1-yl) phosphonic acid: A new class of iron corrosion inhibitors in sodium chloride 3% media. *Appl. Surf. Sci.* **2006**, *252* (18), 6162–6172.
- Wang, P.; Klein, C.; Humphrey-Baker, R.; Zakeeruddin, S. M.; Gratzel, M. Stable $\geq 8\%$ efficient nanocrystalline dye-sensitized solar cell based on an electrolyte of low volatility. *Appl. Phys. Lett.* **2005**, *86* (12), 123508.
- Lee, Y. L.; Huang, B. M.; Chien, H. T. Highly efficient CdSe-sensitized TiO₂ photoelectrode for quantum-dot-sensitized solar cell applications. *Chem. Mater.* **2008**, *20* (22), 6903–6905.
- Monson, T. C.; Lloyd, M. T.; Olson, D. C.; Lee, Y. J.; Hsu, J. W. P. Photocurrent enhancement in polythiophene- and alkanethiol-modified ZnO solar cells. *Adv. Mater.* **2008**, *20* (24), 4755.
- Ogata, K.; Hama, T.; Hama, K.; Koike, K.; Sasa, S.; Inoue, M.; Yano, M. Characterization of alkanethiol/ZnO structures by X-ray photoelectron spectroscopy. *Appl. Surf. Sci.* **2005**, *241* (1–2), 146–149.
- Sadik, P. W.; Pearton, S. J.; Norton, D. P.; Lambers, E.; Ren, F. Functionalizing Zn- and O-terminated ZnO with thiols. *J. Appl. Phys.* **2007**, *101* (10), 104514.
- Taratula, O.; Galoppini, E.; Wang, D.; Chu, D.; Zhang, Z.; Chen, H. H.; Saraf, G.; Lu, Y. C. Binding studies of molecular linkers to ZnO and MgZnO nanoparticle films. *J. Phys. Chem. B* **2006**, *110* (13), 6506–6515.
- Schreiber, F. Structure and growth of self-assembling monolayers. *Prog. Surf. Sci.* **2000**, *65* (5–8), 151–256.
- Kang, M. S.; Ma, H.; Yip, H. L.; Jen, A. K. Y. Direct surface functionalization of indium tin oxide via electrochemically induced assembly. *J. Mater. Chem.* **2007**, *17* (33), 3489–3492.
- Rhodes, C. L.; Lappi, S.; Fischer, D.; Sambasivan, S.; Genzer, J.; Franzen, S. Characterization of monolayer formation on aluminum-doped zinc oxide thin films. *Langmuir* **2008**, *24* (2), 433–440.
- Block, E., *Reactions of Organosulfur Compounds*. Academic Press: New York, 1978.
- Marsden, C. J. Altruism revisited—gas electron-diffraction study of tris(trifluoromethyl)phosphine oxide, Op(CF₃)₃, and ab initio molecular-orbital calculations on X3c-Y and X3c-Y(O) systems (X = H, F - Y = Ph₂, Sh, Cl). *Inorg. Chem.* **1984**, *23* (12), 1703–1708.
- Fukaya, H.; Ono, T.; Abe, T. Bond dissociation energies of CF₃-X bonds (X = C, O, N, S, Br): Ab initio molecular orbital calculation and

- application to evaluation of fire suppression ability. *J. Phys. Chem. A* **2001**, *105* (31), 7401–7404.
- (21) Quin, L. D. *A Guide to Organophosphorus Chemistry*. Wiley: New York, 2000.
- (22) Van Hal, P. A.; Smits, E. C. P.; Geuns, T. C. T.; Akkerman, H. B.; De Brito, B. C.; Perissinotto, S.; Lanzani, G.; Kronemeijer, A. J.; Geskin, V.; Cornil, J.; Blom, P. W. M.; De Boer, B.; De Leeuw, D. M. Upscaling, integration and electrical characterization of molecular junctions. *Nat. Nanotechnol.* **2008**, *3* (12), 749–754.
- (23) Strong, L.; Whitesides, G. M. Structures of self-assembled monolayer films of organosulfur compounds adsorbed on gold single-crystals - electron-diffraction studies. *Langmuir* **1988**, *4* (3), 546–558.
- (24) Dubois, L. H.; Zegarski, B. R.; Nuzzo, R. G. Molecular ordering of organosulfur compounds on Au(111) and Au(100) - adsorption from solution and in ultrahigh-vacuum. *J. Chem. Phys.* **1993**, *98* (1), 678–688.
- (25) Bain, C. D.; Troughton, E. B.; Tao, Y. T.; Evall, J.; Whitesides, G. M.; Nuzzo, R. G. Formation of monolayer films by the spontaneous assembly of organic thiols from solution onto gold. *J. Am. Chem. Soc.* **1989**, *111* (1), 321–335.
- (26) Yang, H. C.; Aoki, K.; Hong, H. G.; Sackett, D. D.; Arendt, M. F.; Yau, S. L.; Bell, C. M.; Mallouk, T. E. Growth and characterization of metal(Ii) alkanebisphosphonate multilayer thin-films on gold surfaces. *J. Am. Chem. Soc.* **1993**, *115* (25), 11855–11862.
- (27) Gao, W.; Dickinson, L.; Grozinger, C.; Morin, F. G.; Reven, L. Self-assembled monolayers of alkylphosphonic acids on metal oxides. *Langmuir* **1996**, *12* (26), 6429–6435.
- (28) Spori, D. M.; Venkataraman, N. V.; Tosatti, S. G. P.; Durmaz, F.; Spencer, N. D.; Zurcher, S. Influence of alkyl chain length on phosphate self-assembled monolayers. *Langmuir* **2007**, *23* (15), 8053–8060.
- (29) Jagadish, C.; Pearton, S. J., *Zinc Oxide Bulk, Thin Films and Nanostructures: Processing, Properties and Applications*. Elsevier: Amsterdam; Boston, 2006; p ix, 589.
- (30) Brewer, S. H.; Brown, D. A.; Franzen, S. Formation of thiolate and phosphonate adlayers on indium-tin oxide: Optical and electronic characterization. *Langmuir* **2002**, *18* (18), 6857–6865.
- (31) Gardner, T. J.; Frisbie, C. D.; Wrighton, M. S. Systems for orthogonal self-assembly of electroactive monolayers on Au and ITO - an approach to molecular electronics. *J. Am. Chem. Soc.* **1995**, *117* (26), 6927–6933.
- (32) Perkins, C. L. A liquid-phase quartz crystal microbalance for photovoltaics research. In *Proceedings of the 33rd IEEE Photovoltaics Specialists Conference*; San Diego, CA, 2008.
- (33) *EF-Micro*; Dainippon Ink and Chemicals, Inc.
- (34) *FC-550 & CHT100, INFICON*; Maxtek, In.
- (35) Masterflex L/S digital drive, P/N EW-07550-50, Cole-Parmer.
- (36) Sun, J. C.; Bian, J. M.; Liang, H. W.; Zhao, J. Z.; Hu, L. Z.; Zhao, Z. W.; Liu, W. F.; Du, G. T. Realization of controllable etching for ZnO film by NH4Cl aqueous solution and its influence on optical and electrical properties. *Appl. Surf. Sci.* **2007**, *253* (11), 5161–5165.
- (37) *RQCM, INIFICON*; Maxtek.
- (38) *P/N EW-01356-16*; Cole-Parmer.
- (39) *CoolCube, P/N R-01356-52*; Cole-Parmer.
- (40) Witt, D.; Klajn, R.; Barski, P.; Grzybowski, B. A. Applications properties and synthesis of omega-functionalized *n*-alkanethiols and disulfides - the building blocks of self-assembled monolayers. *Curr. Org. Chem.* **2004**, *8* (18), 1763–1797.
- (41) Hanson, E. L.; Schwartz, J.; Nickel, B.; Koch, N.; Danisman, M. F. Bonding self-assembled, compact organophosphonate monolayers to the native oxide surface of silicon. *J. Am. Chem. Soc.* **2003**, *125* (51), 16074–16080.
- (42) Perkins, C. L.; Hasoon, F. S. Surfactant-assisted growth of CdS thin films for photovoltaic applications. *J. Vac. Sci. Technol., A* **2006**, *24* (3), 497–504.
- (43) NIST Electron Inelastic-Mean-Free-Path Database v1.1.
- (44) Aqua, T.; Cohen, H.; Vilan, A.; Naaman, R. Long-range substrate effects on the stability and reactivity of thiolated self-assembled monolayers. *J. Phys. Chem. C* **2007**, *111* (44), 16313–16318.
- (45) Hesse, R.; Streubel, P.; Szargan, R. Product or sum: Comparative tests of Voigt, and product or sum of Gaussian and Lorentzian functions in the fitting of synthetic Voigt-based X-ray photoelectron spectra. *Surf. Interface Anal.* **2007**, *39* (5), 381–391.
- (46) Henrich, V. E.; Cox, P. A. *The surface science of metal oxides*. Cambridge University Press: Cambridge; New York, 1994.
- (47) Moulder, J. F. S. W. F.; Sobol, P. E.; Bomben, K. D. *Handbook of X-ray Photoelectron Spectroscopy*; Perkin-Elmer Corporation: Eden Prairie, 1992.
- (48) Castner, D. G.; Hinds, K.; Grainger, D. W. X-ray photoelectron spectroscopy sulfur 2p study of organic thiol and disulfide binding interactions with gold surfaces. *Langmuir* **1996**, *12* (21), 5083–5086.
- (49) We are grateful to Sheyu Guo and EPV Solar for providing ZnO: Al/glass samples. Films were deposited via their proprietary hollow cathode reactive sputtering process.
- (50) Porter, M. D.; Bright, T. B.; Allara, D. L.; Chidsey, C. E. D. Spontaneously organized molecular assemblies 0.4. Structural characterization of normal-alkyl thiol monolayers on gold by optical ellipsometry, infrared-spectroscopy, and electrochemistry. *J. Am. Chem. Soc.* **1987**, *109* (12), 3559–3568.
- (51) Hedberg, J.; Leygraft, C.; Cimatu, K.; Baldelli, S. Adsorption and structure of octadecanethiol on zinc surfaces as probed by sum frequency generation spectroscopy, imaging, and electrochemical techniques. *J. Phys. Chem. C* **2007**, *111* (47), 17587–17596.
- (52) Fontes, G. N.; Neves, B. R. A. Effects of substrate polarity and chain length on conformational and thermal properties of phosphonic acid self-assembled bilayers. *Langmuir* **2005**, *21* (24), 11113–11118.
- (53) Love, J. C.; Wolfe, D. B.; Haasch, R.; Chabinyc, M. L.; Paul, K. E.; Whitesides, G. M.; Nuzzo, R. G. Formation and structure of self-assembled monolayers of alkanethiolates on palladium. *J. Am. Chem. Soc.* **2003**, *125* (9), 2597–2609.
- (54) Wong, E. L. S.; James, M.; Chilcott, T. C.; Coster, H. G. L. Characterisation of alkyl-functionalised Si(111) using reflectometry and AC impedance spectroscopy. *Surf. Sci.* **2007**, *601* (24), 5740–5743.
- (55) Lin, L. Y.; Kim, H. J.; Kim, D. E. Wetting characteristics of ZnO smooth film and nanowire structure with and without OTS coating. *Appl. Surf. Sci.* **2008**, *254* (22), 7370–7376.
- (56) Dedova, T.; Klauson, J.; Badre, C.; Pauporte, T.; Nisumaa, R.; Mere, A.; Volobujeva, O.; Krunks, M. Chemical spray deposition of zinc oxide nanostructured layers from zinc acetate solutions. *Phys. Status Solidi A* **2008**, *205* (10), 2355–2359.
- (57) Kunat, M.; Girol, S. G.; Burghaus, U.; Woll, C. The interaction of water with the oxygen-terminated, polar surface of ZnO. *J. Phys. Chem. B* **2003**, *107* (51), 14350–14356.
- (58) Adolphi, B.; Jahne, E.; Busch, G.; Cai, X. D. Characterization of the adsorption of omega-(thiophene-3-yl alkyl) phosphonic acid on metal oxides with AR-XPS. *Anal. Bioanal. Chem.* **2004**, *379* (4), 646–652.
- (59) Textor, M.; Ruiz, L.; Hofer, R.; Rossi, A.; Feldman, K.; Hahner, G.; Spencer, N. D. Structural chemistry of self-assembled monolayers of octadecylphosphoric acid on tantalum oxide surfaces. *Langmuir* **2000**, *16* (7), 3257–3271.
- (60) Luschnitz, R.; Frenzel, J.; Milek, T.; Seifert, G. Adsorption of phosphonic acid at the TiO₂ anatase (101) and rutile (110) surfaces. *J. Phys. Chem. C* **2009**, *113* (14), 5730–5740.
- (61) Luschnitz, R.; Oliveira, A. F.; Frenzel, J.; Joswig, J. O.; Seifert, G.; Duarte, H. A. Adsorption of phosphonic and ethylphosphonic acid on aluminum oxide surfaces. *Surf. Sci.* **2008**, *602* (7), 1347–1359.
- (62) Dvorak, J.; Jirsak, T.; Rodriguez, J. A. Fundamental studies of desulfurization processes: Reaction of methanethiol on ZnO and Cs/ZnO. *Surf. Sci.* **2001**, *479* (1–3), 155–168.
- (63) Gouzman, I.; Dubey, M.; Carolus, M. D.; Schwartz, J.; Bernasek, S. L. Monolayer vs. multilayer self-assembled alkylphosphonate films: X-ray photoelectron spectroscopy studies. *Surf. Sci.* **2006**, *600* (4), 773–781.
- (64) Halevi, B.; Vohs, J. M. TPD study of the reaction of CH₃CH₂SH and (CH₃CH₂)₂S-2 on ZnO(0001) and ZnO. *Catal. Lett.* **2006**, *111* (1–2), 1–4.
- (65) Lai, Y. H.; Yeh, C. T.; Cheng, S. H.; Liao, P.; Hung, W. H. Adsorption and thermal decomposition of alkanethiols on Cu(110). *J. Phys. Chem. B* **2002**, *106* (21), 5438–5446.
- (66) Huang, T. P.; Lin, T. H.; Teng, T. F.; Lai, Y. H.; Hung, W. H. Adsorption and thermal reaction of short-chain alkanethiols on GaAs(100). *Surf. Sci.* **2009**, *603* (9), 1244–1252.
- (67) Shih, J. J.; Liao, Y. H.; Kuo, K. H.; Lin, J. L. Thermal reactions of mercaptoethanol on Cu(100). *Surf. Sci.* **2005**, *575* (1–2), 163–170.
- (68) Carbonell, L.; Whelan, C. M.; Kinsella, M.; Maex, K. A thermal stability study of alkane and aromatic thiolate self-assembled monolayers on copper surfaces. *Superlattices Microstruct.* **2004**, *36* (1–3), 149–160.
- (69) Menaa, B.; Shannon, I. J. Modulation of the intercalation properties of copper-zinc mixed-metal phosphonate materials. *Chem.–Eur. J.* **2002**, *8* (21), 4884–4893.
- (70) Poojary, D. M.; Zhang, B. L.; Clearfield, A. Syntheses and X-ray powder structures of two zinc propylenebis(phosphonates). *Chem. Mater.* **1999**, *11* (2), 421–426.
- (71) Gerbier, P.; Guerin, C.; Henner, B.; Unal, J. R. An organometallic route to zinc phosphonates and their intercalates. *J. Mater. Chem.* **1999**, *9* (10), 2559–2565.
- (72) Pickett, N. L.; Lawson, S.; Thomas, W. G.; Riddell, F. G.; Foster, D. F.; Cole-Hamilton, D. J.; Fryer, J. R. Gas-phase formation of zinc/cadmium chalcogenide cluster complexes and their solid-state thermal decomposition to form II-VI nanoparticulate material. *J. Mater. Chem.* **1998**, *8* (12), 2769–2776.
- (73) Rees, W. S.; Krauter, G. Preparation and characterization of several group 12 element (Zn, Cd)-bis(thiolate) complexes and evaluation of their potential as precursors for 12–16 semiconducting materials. *J. Mater. Res.* **1996**, *11* (12), 3005–3016.

- (74) Kempe, M. D.; Jorgensen, G. J.; Terwilliger, K. M.; McMahon, T. J.; Kennedy, C. E.; Borek, T. T. Acetic acid production and glass transition concerns with ethylene-vinyl acetate used in photovoltaic devices. *Sol. Energy Mater. Sol. Cells* **2007**, *91* (4), 315–329.
- (75) Ovchenkov, Y. A.; Geisler, H.; Burst, J. M.; Thornburg, S. N.; Ventrice, C. A.; Zhang, C. J.; Redepenning, J.; Losovyj, Y.; Rosa, L.; Dowben, P. A.; Doudin, B. The electronic structure of metal/alkane thiol self-assembled monolayers/metal junctions for magnetoelectronics applications. *Chem. Phys. Lett.* **2003**, *381* (1–2), 7–13.
- (76) Katz, H. E.; Johnson, J.; Lovinger, A. J.; Li, W. J. Naphthalene-tetracarboxylic diimide-based *n*-channel transistor semiconductors: Structural variation and thiol-enhanced gold contacts. *J. Am. Chem. Soc.* **2000**, *122* (32), 7787–7792.
- (77) Lu, C. S.; Lewis, O. Investigation of Film-Thickness Determination by Oscillating Quartz Resonators with Large Mass Load. *J. Appl. Phys.* **1972**, *43* (11), 4385–4390.

JP906013R